PAPER

Resolution and stability analysis in acousto-electric imaging

Inverse Problems **28** (2012) 084005 (20pp) doi:10.1088/0266-5611/28/8/084005

Resolution and stability analysis in acousto-electric imaging

Habib Ammari[1], **Josselin Garnier**[2] **and Wenjia Jing**[1]

[1] Département de Mathématiques et Applications, Ecole Normale Supérieure, 45 Rue d'Ulm, 75005 Paris, France
[2] Laboratoire de Probabilités et Modèles Aléatoires & Laboratoire Jacques-Louis Lions, Université Paris VII, 2 Place Jussieu, 75251 Paris Cedex 5, France

E-mail: habib.ammari@ens.fr, garnier@math.jussieu.fr and wjing@dma.ens.fr

Received 14 December 2011, in final form 30 April 2012
Published 30 July 2012
Online at stacks.iop.org/IP/28/084005

Abstract
We consider the optimization approach to the acousto-electric imaging problem. Assuming that the electric conductivity distribution is a small perturbation of a constant, we investigate the least-squares estimate analytically using (multiple) Fourier series, and confirm the widely observed fact that acousto-electric imaging has high resolution and is statistically stable. We also analyze the case of partial data and the case of limited-view data, in which some singularities of the conductivity can still be imaged.

(Some figures may appear in colour only in the online journal)

1. Introduction

The acousto-electric imaging (AEI) is a hybrid technique that combines classical electrical impedance tomography (EIT) and ultrasound to reconstruct the internal electric conductivity of a body. It can be cast as the inverse problem that aims to find the coefficient of an elliptic equation from interior data [1].

The precise mathematical model is as follows. Let $X \subset \mathbb{R}^2$ represent the body with the conductivity distribution $\gamma(x)$. The voltage u and the current field $\gamma\nabla u$ satisfy

$$\begin{aligned} &\nabla \cdot \gamma(x)\nabla u(x) = 0, \quad x \in X, \\ &\gamma(x)\frac{\partial u}{\partial n}(x) = g(x), \quad x \in \partial X. \end{aligned} \tag{1.1}$$

Here, the Neumann boundary condition $\gamma\partial_n u = g$ represents some electric currents injected at the boundary. We assume that g integrates into zero over the boundary, and that u integrates to zero over X. Other boundary conditions such as Dirichlet or Robin boundary conditions can also be considered.

AEI aims to reconstruct $\gamma(x)$ from measurements consisting of electric power density distributions inside the body, that is,

$$\{H(x) = \gamma(x)|\nabla u(x)|^2 : x \in X\}. \tag{1.2}$$

These data are internal; however, they are constructed from differential boundary measurements. We will briefly review the acquisition of these data in the next section. Therefore, AEI is non-intrusive and harmless. We refer the reader to [17] for the physics background and practical implementations of AEI, and to [1, 2, 10, 11] for mathematical formulations.

The uniqueness of AEI in two dimensions with two proper datasets was obtained in [9], and was generalized to three and higher dimensions in [7, 8]. The latter papers contain stability estimates as well. The reconstruction procedures in these papers involve solving systems of transport equations and have been implemented in [14].

A numerical scheme based on optimization and zero-Laplacian equation, which results from substituting the relation $H = \gamma|\nabla u|^2$ into (1.1), was considered in [2]; another optimization algorithm based on minimizing the power density discrepancy was developed in [9]. Convergence and stability analysis of these schemes, however, are open questions in the general case.

In this paper, we analyze AEI in the linearized regime, i.e. the conductivity distribution is a small perturbation of some constant background γ_0 or $\gamma(x) = (1 + \varepsilon\rho(x))\gamma_0$. Such a regime was considered in [12] where the authors reconstructed ρ by solving a Poisson equation, and their approach required differentiating the data. We take the optimization approach similar to [9]; however, we take into account not only the power density distributions $\gamma|\nabla u_1|^2$ and $\gamma|\nabla u_2|^2$, where u_1 and u_2 correspond to two Neumann data g_1 and g_2 such that ∇u_1 and ∇u_2 are not parallel in X, but also the cross density distribution $\gamma\nabla u_1 \cdot \nabla u_2$. This 'additional' information turns out to be important. On the unit two-dimensional square and using two proper datasets, we obtain an explicit reconstruction formula based on the least-squares solution. Our analysis characterizes the Fourier modes of the reconstruction, and the effects of additive measurement noise in the data. This analysis is in the same spirit as [5, 6], and our result shows that the resolving power of the measurements is infinite. In other words, we may say that AEI has super resolution. The results proved here may be extended to the nonconstant background conductivity case using pseudo-differential techniques. In this direction, we refer to [13]. It is also expected that they can be generalized to other imaging modalities from internal measurements such as magnetic resonance EIT [15], quantitative thermo-acoustic imaging [4] and microwave imaging by elastic perturbations [3, 16].

2. Formulation of the problem

In this section, we formulate the optimization approach to the AEI problem. We start by briefly reviewing the acquisition of internal power density distributions; this is in fact the first step of AEI. Then we introduce the optimization functional and outline the analysis of its least-squares solution. Finally, we investigate the linearization of the optimization functional.

Throughout the paper, $\|\cdot\|_{p,A}$ denotes the L^p norm of a function over a set A. When p equals two or the set A is obvious from the context, the corresponding labels are ignored.

2.1. Acquisition of the power density distributions

As mentioned earlier, AEI uses internal data that are obtained from non-intrusive measurements. This is possible due to the combination of ultrasound and EIT.

Similar to EIT, AEI measures the voltage response to one or several current injections at the boundary. The number of injected currents we need in this paper is d, the same as the dimension of the body X. For simplicity, we assume $d = 2$ throughout the paper. Let g_j, $j = 1, 2$ be the current pattern applied at the boundary, and $\psi_j = u_j|_{\partial X}$ be the corresponding voltage response at the boundary. These measurements are exactly as those of the classical EIT. What distinguishes AEI from EIT is that it requires another measurement: the boundary voltage response to g_j when an ultrasound beam is focused at an internal point $z \in X$. Let $\psi_j(\cdot; z)$ denote such a response. Consequently, the measurements of AEI consist of

$$\{(g_j(x), \psi_j(x; z) - \psi_j(x)) : x \in \partial X, z \in X\}.$$

From these measurements, one can form the matrix

$$H_{jk}(z) := \int_{\partial X} g_j(x)[\psi_k(x; z) - \psi_k(x))]\,\mathrm{d}x. \tag{2.1}$$

Throughout the paper, the roman indices j, k, etc run from one to two if not otherwise stated. The difference between $\psi_j(x; z)$ and $\psi_j(x)$ is due to the electro-acoustic effect, i.e. the ultrasound focusing at z changes the conductivity distribution slightly near z. Asymptotic analysis shows that $H_{jk}(z)$ is well approximated by $\gamma(z)\nabla u_j(z) \cdot \nabla u_k(z)$ (for smooth γ); see [2].

Henceforth, our data are the matrix $H(x) = \{H_{jk}(x) = \gamma(x)\nabla u_j(x) \cdot \nabla u_k(x)\}$. Note that H_{11} and H_{22} are the power density distributions corresponding to the two currents g_1 and g_2, respectively.

2.2. Outline of the optimization approach

Define the admissible set of the conductivity distribution to be

$$L^{\infty}_{\beta_1,\beta_2} := \{0 < \beta_1 < \gamma(x) < \beta_2 < \infty \text{ for } x \in X\}, \tag{2.2}$$

for some positive real numbers $\beta_1 < \beta_2$. Let $u_j[\gamma]$ be the map from γ to the solution of (1.1) with boundary current g_j. Let $F_{jk}[\gamma]$ be the map from γ to the cross power density function $\gamma\nabla u_j[\gamma] \cdot \nabla u_k[\gamma]$.

Let $F[\gamma](\cdot)$ denote the matrix formed by $F_{jk}[\gamma](\cdot)$. Denote by $|||\cdot|||$ the Hilbert–Schmidt norm of a matrix. Then the optimization approach to AEI is to find

$$\gamma_* = \arg\min J[\gamma] = \arg\min \frac{1}{2}\int_X |||F[\gamma](x) - H(x)|||^2\,\mathrm{d}x. \tag{2.3}$$

The map $F_{jk}[\gamma]$ is highly nonlinear. In the linearized regime, when $\gamma = \gamma_0(1 + \varepsilon\rho)$, we can linearize this map and write

$$F_{jk}[\gamma] \approx F_{jk}[\gamma_0] + \mathcal{D}F_{jk}[\gamma_0](\gamma - \gamma_0),$$

where $\mathcal{D}F_{jk}[\gamma_0]$ is the Fréchet derivative of the data map. If we substitute this linearization into the functional, $J[\gamma]$ can be approximated by a quadratic form in $\gamma - \gamma_0$. The least-squares solution of the approximated functional is then given by $\gamma_* \approx \gamma_0 + \rho_*$, where ρ_* satisfies

$$\sum_{j,k=1}^{2} \mathcal{D}F_{jk}[\gamma_0]^*\mathcal{D}F_{jk}[\gamma_0](\rho_*) = \sum_{j,k=1}^{2} \mathcal{D}F^*_{jk}[\gamma_0](H_{jk} - F_{jk}[\gamma_0]). \tag{2.4}$$

Here, $\mathcal{D}F^*[\gamma_0]$ is the formal adjoint of $\mathcal{D}F[\gamma_0]$.

Observe that u_j and hence F_{jk} depend on the boundary conditions (also known as illuminations). If the illuminations are chosen properly so that the operator on the left-hand side of the above equation is invertible, then ρ_* can be found and $\gamma_0 + \rho_*$ serves as an approximation of γ_*. In section 3, we will provide such illuminations and discuss the quality of the above reconstruction method.

2.3. The linearized conductivity problem

In the linearized regime, where $\gamma = (1+\rho)\gamma_0$ and $\|\rho\|_\infty$ is small, according to the optimization approach outlined above, we need to investigate the Fréchet derivative $\mathcal{D}F_{jk}[\gamma_0]$. The goal of this section is to find the expressions for this operator and its adjoint. It is obvious that these operators are closely related to the Fréchet derivative of $u_j[\gamma]$, so we shall find its expression as well. Since (2.4) only requires derivative at γ_0, we will abuse notation a little bit and denote by $\mathcal{D}u$ and $\mathcal{D}F_{jk}$ their values at γ_0.

Our analysis in the next two sections is based on Fourier series, and it is most convenient when the body X is the unit square and the conductivity problem is equipped with periodic conditions. So we set $X = (0, 1)^2$, assume that supp $\rho \subset\subset X$ and identify its closure with the two torus $\mathbb{T}^2$.

Let $\mathcal{C}(\mathbb{T}^2)$ denote the space of real-valued functions that are continuous on $\mathbb{T}^2$, and define $\mathcal{C}^m(\mathbb{T}^2)$ and $\mathcal{C}^\infty(\mathbb{T}^2)$, accordingly. Define $L^p(\mathbb{T}^2)$, $1 \leqslant p \leqslant \infty$, to be the completion of $\mathcal{C}^\infty(\mathbb{T}^2)$ with respect to the L^p-norm. Furthermore, define the Sobolev space $W^{k,p}(\mathbb{T}^2)$ in a similar way. The Poincaré inequality does not hold for a function in $W^{1,2}(\mathbb{T}^2)$; however, it holds if we remove the average of the function. Therefore, we define

$$W(\mathbb{T}^2) := \left\{ \varphi \in W^{1,2}(\mathbb{T}^2) \Big| \int_{\mathbb{T}^2} \varphi = 0 \right\}. \tag{2.5}$$

We modify the definition of the admissible set to

$$L^\infty_{\beta_1,\beta_2}(\mathbb{T}^2) := L^\infty_{\beta_1,\beta_2}(X) \bigcap L^\infty(\mathbb{T}^2). \tag{2.6}$$

Now let us equip the conductivity problem (1.1) with periodic boundary conditions.

Let ψ_j, $j = 1, 2$, be two functions in $\mathcal{C}^1(X)$ such that $\nabla\psi_j \in \mathcal{C}(\mathbb{T}^2)$. In practice, we will choose linear functions for which $\nabla\psi_j$ is constant. The periodic condition we impose on $u_j[\gamma]$ is

$$u_j - \psi_j \in W^{1,2}(\mathbb{T}^2). \tag{2.7}$$

If we set $\tilde{u}_j[\gamma] = u_j[\gamma] - \psi_j$, then it is the unique function in W that satisfies

$$\int_{\mathbb{T}^2} \gamma\nabla\tilde{u}_j[\gamma]\cdot\nabla\varphi = \int_{\mathbb{T}^2} \varphi\nabla\cdot(\gamma\nabla\psi_j), \quad \forall\varphi \in W(\mathbb{T}^2). \tag{2.8}$$

The existence and uniqueness of the above problem are due to the fact that $\nabla\cdot(\gamma\nabla\psi)$ averages to zero over the square. We observe that the derivative of $u_j[\gamma]$ is the same as that of $\tilde{u}_j[\gamma]$.

Let us view the map $\tilde{u}_j$ as

$$\begin{array}{rccc} \tilde{u}_j[\gamma]: & L^\infty_{\beta_1,\beta_2}(\mathbb{T}^2) & \to & W(\mathbb{T}^2) \\ & \gamma & \mapsto & \tilde{u}_j[\gamma]. \end{array}$$

The following lemma characterizes the expression of $\mathcal{D}u_j$ at γ_0.

Lemma 2.1. *The Fréchet derivative of $u_j[\gamma]$ at γ_0 is the map from $L^\infty(\mathbb{T}^2)$ to $W(\mathbb{T}^2)$ given by $\mathcal{D}u_j(\rho) = v_j[\rho]$, where $v_j[\rho]$ is the weak solution of the following problem:*

$$\begin{aligned} &\nabla\cdot\gamma_0\nabla v_j[\rho] = -\nabla\cdot\left(\rho\nabla u_0^j\right), \quad x \in X, \\ &v_j[\rho] \in W(\mathbb{T}^2). \end{aligned} \tag{2.9}$$

Here, u_0^j solves (1.1) with the background conductivity distribution γ_0 and the aforementioned periodic condition (2.7).

Proof. It suffices to show that for $\|\rho\|_\infty$ sufficiently small,

$$\|\tilde{u}_j[\gamma_0+\rho](\cdot)-\tilde{u}_0^j(\cdot)-v_j[\rho](\cdot)\|_{W^{1,2}} \leqslant C\|\rho\|_\infty^{1+r}, \tag{2.10}$$

for some positive r. Recall (2.8) and a similar weak formulation for v_j. We find

$$\int_X (\gamma_0+\rho)\big(\nabla\tilde{u}_j[\gamma_0+\rho]-\nabla\tilde{u}_0^j-\nabla v_j[\rho]\big)\cdot\nabla\varphi\,\mathrm{d}x = -\int_X \rho\nabla v_j[\rho]\cdot\nabla\varphi\,\mathrm{d}x,$$

for all $\varphi\in W(\mathbb{T}^2)$. Take $\varphi=\tilde{u}_j[\gamma_0+\rho]-\tilde{u}_0^j-v_j[\rho]$. Suppose that $\|\rho\|_\infty$ is sufficiently small and verifies $\gamma_0+\rho\in L^\infty_{\beta_1,\beta_2}(\mathbb{T}^2)$. Then the standard estimate yields

$$\|\nabla\tilde{u}_j[\gamma_0+\rho]-\nabla\tilde{u}_0^j-\nabla v_j[\rho]\| \leqslant \beta_2\beta_1^{-1}\|\rho\|_\infty\|\nabla v_j[\rho]\|.$$

The same argument applied to problem (2.9) yields $\|\nabla v_j[\rho]\| \leqslant C\|\rho\|_\infty\|\nabla u_0^j\|$. Since $u_j[\gamma_0+\rho]-u_0^j-v_j[\rho]$ is an element of $W(\mathbb{T})$ and Poincaré's inequality applies in this space, the above estimate shows that (2.10) holds with $r=1$. □

We reiterate that (2.9) is well posed because the right-hand side averages to zero over X, thanks to the fact that ρ and $\partial_k u_0^j$ are all periodic. The characterization of $\mathcal{D}F_{jk}$ is now an immediate consequence of the above lemma.

Lemma 2.2. *Assume that u_0^j belongs to $W^{1,\infty}(X)$. Then the Fréchet derivative of F_{jk} at γ_0 is a linear map from $L^\infty(\mathbb{T}^2)$ to $L^2(\mathbb{T}^2)$ given by*

$$\mathcal{D}F_{jk}(\rho) := \rho\nabla u_0^j\cdot\nabla u_0^k+\gamma_0\nabla u_0^j\cdot\nabla v_k[\rho]+\gamma_0\nabla v_j[\rho]\cdot\nabla u_0^k. \tag{2.11}$$

Here, $v_k[\rho]$ and u_0^k are defined as in lemma 2.1. Moreover,

$$\|F_{jk}[\gamma_0+\rho]-F_{jk}[\gamma_0]-\mathcal{D}F_{jk}(\rho)\| \leqslant C\|\rho\|_\infty^2. \tag{2.12}$$

Furthermore, the domain of $\mathcal{D}F_{jk}$ can be extended to $L^2(\mathbb{T}^2)$, and we have

$$\|\mathcal{D}F_{jk}(\rho)\| \leqslant C\|\rho\|. \tag{2.13}$$

The above constants C in (2.12) and (2.13) depend on the elliptic coefficients β_1 and β_2, the volume of the domain X, and the $W^{1,\infty}$-norms of u_0^j and u_0^k.

Proof. According to the previous lemma, $u_j[\gamma_0+\rho]$ (and similarly u_k) can be written as $u_0^j+v_j[\rho]+s_j$, with $\|\nabla s_j\| \leqslant C\|\rho\|_\infty^2$. Using this decomposition, we verify that $F_{jk}[\gamma_0+\rho]-F_{jk}[\gamma_0]-\mathcal{D}F_{jk}(\rho)$ consists of products of at least two elements of the set $\{\rho,\nabla v_j[\rho],\nabla v_k[\rho],\nabla s_j,\nabla s_k\}$. Since all of them are bounded by $C\|\rho\|_\infty$, estimate (2.12) holds. This also verifies the expression of $\mathcal{D}F_{jk}$. To see that the range of $\mathcal{D}F_{jk}$ is in $L^2(\mathbb{T}^2)$, we observe that $\partial_k u_0^j$ is periodic.

Estimate (2.13) is easily seen from the expression of $\mathcal{D}F_{jk}$ and the estimate $\|\nabla v_j[\rho]\| \leqslant C\|\nabla u_0^j\|_\infty\|\rho\|$. □

Let us extend the domain of $\mathcal{D}F_{jk}$ to $L^2(\mathbb{T}^2)$, which is a Hilbert space. Then the adjoint operator $\mathcal{D}F_{jk}^*$ is defined by the relation

$$\langle\mathcal{D}F_{jk}(\rho),\phi\rangle = \langle\rho,\mathcal{D}F_{jk}^*(\phi)\rangle, \quad \forall\rho,\varphi\in L^2(\mathbb{T}^2). \tag{2.14}$$

Here, $\langle\,\rangle$ denotes the L^2-scalar product. It is now a simple task of integration by parts to check that $\mathcal{D}F_{jk}$ is self-adjoint, that is, $\mathcal{D}F_{jk}^*(\phi)$ verifies the same expression (2.11).

Remark 2.3. The above formulation works for Dirichlet and Neumann boundary conditions as well. In fact, $\mathcal{D}u_j$ and $\mathcal{D}F_{jk}$ will have the same expressions but the boundary condition for v_j and the domain of these operators need to be modified accordingly. We will not discuss these slight variations further.

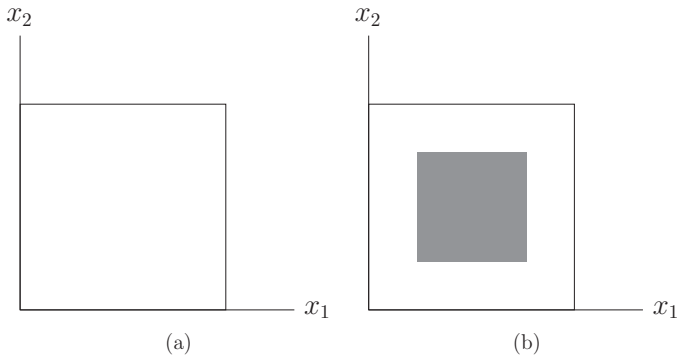

Figure 1. The unit square domain. (a) Data are collected on the whole square. (b) Data are collected on the inner square. In both cases, all four faces of the square are accessible.

3. AEI with full aperture and super resolution

In this and the next sections, we will analyze AEI using Fourier series. As mentioned before, we work on the unit square and impose periodic boundary conditions for the conductivity problem.

The geometric setting of the current problem is as in figure 1. We assume that all four faces of the square are accessible, i.e. we can inject currents or measure voltage imposed there. This is what we mean by the 'full-aperture' case. In this section, we consider the perfect situation when data over the whole square are available; in the next section, we consider a restricted case when data are only available on a partial set, as illustrated in part (b) of the figure.

We recall the basic notions and results of Fourier series on $\mathbb{T}^2$. The set of complex exponentials

$$\{e^{i2\pi\xi\cdot x} : \xi = (\xi_1, \xi_2) \in \mathbb{Z}^2\}$$

forms an orthonormal basis of $L^2(\mathbb{T}^2; \mathbb{C})$. Then the Fourier coefficients of a function f in $\mathcal{C}^\infty(\mathbb{T}^2)$ are given by

$$\mathscr{F}f(\xi) = \int_{\mathbb{T}^2} f(x)\, e^{-i2\pi\xi\cdot x}\, dx, \quad \xi \in \mathbb{Z}^2. \tag{3.1}$$

Conversely, given its Fourier coefficients, a function $f \in \mathcal{C}^\infty(\mathbb{T}^2)$ is recovered by

$$f(x) = \mathscr{F}^*(\mathscr{F}f) = \sum_{\xi\in\mathbb{Z}^2} \mathscr{F}f(\xi)\, e^{i2\pi\xi\cdot x}. \tag{3.2}$$

The definition of $\mathscr{F}$ extends to $L^2(\mathbb{T}^2)$ and $\mathscr{F}^*\mathscr{F} = I$ holds. Recall Parseval's identity

$$\|f\|^2 = \sum_{\xi\in\mathbb{Z}^2} |\mathscr{F}f(\xi)|^2. \tag{3.3}$$

When $f \in W^{1,2}(\mathbb{T}^2)$, we have

$$(\mathscr{F}\partial_j f)(\xi) = i2\pi\xi_j \mathscr{F}f(\xi), \quad j = 1, 2. \tag{3.4}$$

Finally, let us recall the identification

$$W^{k,2}(\mathbb{T}^2) = \left\{ f \in L^2(\mathbb{T}^2) : \sum_{\xi\in\mathbb{Z}^2} \langle\xi\rangle^{2k} |\mathscr{F}f(\xi)|^2 < \infty \right\}, \tag{3.5}$$

where $\langle\xi\rangle = \sqrt{1 + |\xi|^2}$. Furthermore, when $k > 1$, the Sobolev embedding $W^{k,2}(\mathbb{T}^2) \subset L^\infty(\mathbb{T}^2)$ holds. In the following, we also use $\hat{f}$ or $f^\wedge$ to denote $\mathcal{F}f$.

3.1. Reconstruction based on two orthogonal currents

Now we specify our choice of ψ_j in (2.7) and investigate the optimization approach outlined in section 2.2. Without loss of generality, we assume $\gamma_0 = 1$, so that the conductivity distribution is of the form $\gamma = 1 + \rho$ for $\rho \in L^\infty(\mathbb{T}^2)$ and $\|\rho\|_\infty$ is small.

Let $\{\boldsymbol{e}_j : j = 1, 2\}$ be the unit vectors of the two axes. Let $a > 0$ indicate the amplitude of injected currents. We choose ψ_j to be $\psi_j(x) = a\boldsymbol{e}_j \cdot x$. Recall that u_0^j denotes the solution in the homogeneous medium $\gamma_0 = 1$. It follows that

$$u_0^j(x) = \psi_j = a\boldsymbol{e}_j \cdot x, \quad \nabla u_0^j(x) = a\boldsymbol{e}_j.$$

In particular, the expressions of $\mathcal{D}F_{jk}$ and its adjoint simplify to

$$\begin{aligned} \mathcal{D}F_{jk}(\rho) &= a^2\rho\boldsymbol{e}_j \cdot \boldsymbol{e}_k + a\boldsymbol{e}_j \cdot \nabla v_k[\rho] + a\nabla v_j[\rho] \cdot \boldsymbol{e}_k, \\ \mathcal{D}F_{jk}^*(\phi) &= a^2\phi\boldsymbol{e}_j \cdot \boldsymbol{e}_k + a\boldsymbol{e}_j \cdot \nabla w_k[\phi] + a\nabla w_j[\phi] \cdot \boldsymbol{e}_k. \end{aligned} \tag{3.6}$$

Note that $v_j[\rho]$ solves problem (2.9), and $w_k[\phi]$ solves a similar problem with ρ replaced by ϕ. The following result expresses the operator $\mathcal{D}F_{jk}$ in the Fourier domain.

Lemma 3.1. *For any $\rho \in L^2(\mathbb{T}^2)$, we have*

$$(\mathcal{D}F_{jk}(\rho))^\wedge(\xi) = a^2(\boldsymbol{e}_j \cdot \boldsymbol{e}_k - 2(\boldsymbol{e}_j \cdot \tilde{\xi})(\boldsymbol{e}_k \cdot \tilde{\xi}))\hat{\rho}(\xi), \quad \text{for} \quad \xi \neq 0, \tag{3.7}$$

and $(\mathcal{D}F_{jk}(\rho))^\wedge(0) = a^2\boldsymbol{e}_j \cdot \boldsymbol{e}_k\hat{\rho}(0)$. Here, $\tilde{\xi} = \xi/|\xi|$.

Proof. This result follows from a straightforward calculation. Indeed, $v_j[\rho]$ satisfies, in the sense of distributions, equation (2.9) with right-hand side $-a\partial_j\rho$. When $\xi \neq 0$, thanks to (3.4), we have

$$(\nabla v_j[\rho])^\wedge(\xi) = \mathrm{i}2\pi\xi(v_j[\rho])^\wedge(\xi), \quad (\Delta v_j[\rho])^\wedge(\xi) = -4\pi^2|\xi|^2(v_j[\rho])^\wedge(\xi).$$

Similarly, $(-a\partial_j\rho)^\wedge(\xi) = -a(\mathrm{i}2\pi\xi_j)\hat{\rho}(\xi)$. Consequently,

$$(v_j[\rho])^\wedge(\xi) = \mathrm{i}a\frac{2\pi\boldsymbol{e}_j \cdot \xi}{4\pi^2|\xi|^2}\hat{\rho}(\xi).$$

The expression for $(v_k[\rho])^\wedge$ is similar. Consequently, taking Fourier coefficients on both sides and using these expressions, we verify that (3.7) holds.

The case of $\xi = 0$ follows from expression (3.6) and the fact that $\nabla v_j[\rho]$ averages to zero over X. □

Let $\mathcal{Q}$ denote the operator $\sum_{j,k=1,2}\mathcal{D}F_{jk}^*\mathcal{D}F_{jk}$ from $L^2(\mathbb{T}^2)$ onto itself. The following result shows that $\mathcal{Q}$ admits a bounded inverse. In fact, $\mathcal{Q}$ is the identity operator up to a multiplicative constant.

Theorem 3.2. *We have*

$$(\mathcal{Q}\rho)^\wedge(\xi) = 2a^4\hat{\rho}(\xi). \tag{3.8}$$

The reconstruction formula (2.4) then becomes

$$\rho_* = \mathcal{Q}^{-1}\sum_{j,k=1}^{2}\mathcal{D}F_{jk}^*(H_{jk} - F_{jk}[\gamma_0]). \tag{3.9}$$

Furthermore, if $(\varepsilon\rho_r)$ denotes $\gamma_r - \gamma_0$, where γ_r is the true conductivity distribution, then we have

$$\|\rho_* - \varepsilon\rho_r\| \leqslant C\varepsilon^2\|\rho_r\|_\infty^2. \tag{3.10}$$

Proof. The identity in (3.8) can be verified using (3.7). For non-zero ξ, we calculate

$$(\mathcal{Q}\rho)^\wedge(\xi) = a^4\hat{\rho}(\xi)([1-2(\boldsymbol{e}_1\cdot\tilde{\xi})^2]^2 + 2[-2(\boldsymbol{e}_1\cdot\tilde{\xi})(\boldsymbol{e}_2\cdot\tilde{\xi})]^2 + [1-2(\boldsymbol{e}_2\cdot\tilde{\xi})^2]^2)$$
$$= a^4[1+(1-2[(\boldsymbol{e}_2\cdot\tilde{\xi})^2+(\boldsymbol{e}_2\cdot\tilde{\xi})^2])^2]\hat{\rho}(\xi) = 2a^4\hat{\rho}(\xi).$$

We verify that when $\xi = 0$, the above still holds. This proves the first part of the theorem. In fact, it shows that $\mathcal{Q} = 2a^4 I$.

For the second part, we observe that $H(x) = F[\gamma_r]$. Therefore, lemma 2.2 shows that

$$H_{jk} - F_{jk}[\gamma_0] = \sum_{j,k=1}^{2} \mathcal{D}F_{jk}(\varepsilon\rho_r) + E_{jk},$$

where $\|E_{jk}\| \leqslant C\|\varepsilon\rho_r\|_\infty^2$. Substituting this decomposition into the reconstruction formula, we find that

$$\rho_* - \varepsilon\rho_r = \mathcal{Q}^{-1}\sum_{j,k=1}^{2} \mathcal{D}F_{jk}^* E_{jk}.$$

Let $\|\mathcal{Q}^{-1}\|_{\mathcal{L}(L^2,L^2)}$ and $\|\mathcal{D}F_{jk}^*\|_{\mathcal{L}(L^2,L^2)}$ denote the operator norms. Since they are bounded according to (3.8) and (2.13), we have

$$\|\rho_* - \varepsilon\rho_r\| \leqslant \|\mathcal{Q}^{-1}\|_{\mathcal{L}} \sum_{j,k=1}^{2} \|\mathcal{D}F_{jk}^*\|_{\mathcal{L}}\|E_{jk}\| \leqslant C\varepsilon^2\|\rho_r\|_\infty^2. \tag{3.11}$$

This completes the proof. □

Remark 3.3. A more precise estimate of the construction error $\rho_* - \varepsilon\rho_r$ is characterized through Fourier modes. According to the calculations above, we have

$$(\hat{\rho}_* - \varepsilon\hat{\rho}_r)(\xi) = \frac{1}{2a^2}((1-2(\boldsymbol{e}_1\cdot\tilde{\xi})^2)(E_{11})^\wedge(\xi)$$
$$-2(\boldsymbol{e}_1\cdot\tilde{\xi})(\boldsymbol{e}_2\cdot\tilde{\xi})(E_{12}+E_{21})^\wedge(\xi) + (1-(\boldsymbol{e}_2\cdot\tilde{\xi})^2)(E_{22})^\wedge(\xi)), \tag{3.12}$$

for non-zero modes ξ. We also verify that $(\hat{\rho}_* - \varepsilon\hat{\rho}_r)(0) = \frac{1}{2a^2}(\mathscr{F}E_{11} + \mathscr{F}E_{22})(0)$. Since the higher order terms E_{jk} have small L^2 norm, the above formula shows that the reconstruction is quite accurate in all Fourier modes. In this sense, we say that AEI has super resolution.

Remark 3.4. We note that two illuminations are needed for $\mathcal{Q}$ to be invertible. Indeed, suppose that we only use the current $a\boldsymbol{e}_1$; then lemma 3.1 shows

$$(\mathcal{D}F_{11}^*\mathcal{D}F_{11}(\rho))^\wedge(\xi) = 4a^4(1-2(\boldsymbol{e}_1\cdot\tilde{\xi})^2)^2.$$

Therefore, $\mathcal{D}F_{11}^*\mathcal{D}F_{11}$ eliminates Fourier modes which satisfy $\tilde{\xi}\cdot\boldsymbol{e}_1 = \pm 1/\sqrt{2}$, i.e. modes whose directions are separated from $\boldsymbol{e}_1$ by $\pm\pi/4$.

Even when two orthogonal currents are used, the cross information H_{12} and H_{21} is essential. Indeed, the above formula with $\boldsymbol{e}_1$ replaced by $\boldsymbol{e}_2$ applies to the operator $\mathcal{D}F_{22}^*\mathcal{D}F_{22}$. Since $\{|\xi\cdot\boldsymbol{e}_1| = 1/\sqrt{2}\} = |\{\xi\cdot\boldsymbol{e}_2| = 1/\sqrt{2}\}$, the operator $\mathcal{D}F_{22}^*\mathcal{D}F_{22}$ eliminates exactly the same Fourier modes as $\mathcal{D}F_{11}^*\mathcal{D}F_{11}$. The sum of the two still fails to capture these modes.

3.2. The effect of measurement noise

Now we consider additive measurement noise. The noisy data are then written as

$$H^{\mathrm{m}}(x,\omega) = H(x) + V(x;\omega), \tag{3.13}$$

where the superscript 'm' indicates the measured value. The functions H^{m}, H and V all have values in $\mathbb{M}$, the space of 2×2 real symmetric matrices. In particular, we model $V(x;\omega)$ as a $\mathbb{M}$-valued random process on some abstract probability space $(\Omega, \mathcal{F}, \mathbb{P})$ parameterized by $x \in X$. Let $\hat{V}_{jk}(\xi)$ and $\xi \in \mathbb{Z}^2$ denote the Fourier coefficients of the V_{jk}. We assume that the coefficients $\hat{V}_{jk}$ satisfy the following conditions.

(H1) $\hat{V}_{jk}(\xi)$ and $\hat{V}_{rs}(\eta)$ are independent unless $j = r$, $k = s$ and $\xi = \eta$. Furthermore, they are identically distributed Gaussian random variables with mean zero and variance

$$\mathbb{E}|\hat{V}_{jk}(\xi)|^2 = 2\sigma^2 a^2, \quad \xi \in \mathbb{Z}^2, \tag{3.14}$$

where a is the amplitude of the background current. This corresponds to an additive white noise in the measurements as shown below.

(H2) Assume $\varepsilon^2 \ll \sigma \ll \varepsilon$.

Remark 3.5. We justify the above model. Recall the acquisition of the data in (2.1). The additive noise occurs when measuring the differential voltage response $\psi_k(x;z) - \psi_k(x)$. Suppose this function is corrupted by an additive random noise $q_k(x;z,\omega)$. Then according to (2.1), we find

$$V_{jk} = \int_{\partial X} g_j(x) q_k(x,z;\omega)\,\mathrm{d}x.$$

Assume the following holds for the random noise model $q_k(x;z,\omega)$.

(G1) The two processes $q_1(\cdot,\omega)$ and $q_2(\cdot,\omega)$ are independent and identically distributed.

(G2) The process $q_1(x,z;\omega)$ is a white noise on the product space $\partial X \times X$ with variance σ^2. Heuristically, this means for any (x,z) and (x',z') in $\partial X \times X$, we have

$$\mathbb{E}\{q(x,z)q(x',z')\,\mathrm{d}x\,\mathrm{d}x'\,\mathrm{d}z\,\mathrm{d}z'\} = \sigma^2\delta(x-x')\delta(z-z')\,\mathrm{d}x\,\mathrm{d}z\,\mathrm{d}x'\,\mathrm{d}z', \tag{3.15}$$

where δs are the corresponding Dirac measures.

Using the above identity, we verify that

$$\begin{aligned}\mathbb{E}\hat{V}_{jk}(\xi)\overline{\hat{V}_{rs}}(\eta) &= \int_{(\partial X\times X)^2} g_j(x)g_r(x')\,\mathrm{e}^{-\mathrm{i}2\pi\xi\cdot z}\,\mathrm{e}^{\mathrm{i}2\pi\eta\cdot z'}\,\mathbb{E}\{q_k(x,z)q_s(x',z')\,\mathrm{d}x\,\mathrm{d}z\,\mathrm{d}x'\,\mathrm{d}z'\}\\ &= \delta_{ks}\sigma^2\int_{\partial X\times X} g_j(x)g_r(x)\,\mathrm{e}^{-\mathrm{i}2\pi(\xi-\eta)\cdot z}\,\mathrm{d}z\,\mathrm{d}x\\ &= \sigma^2\delta_{ks}\delta_{\xi\eta}\langle g_j, g_r\rangle_{\partial X}.\end{aligned}$$

In the last line, δs are the Kronecker delta functions. Recall that the boundary currents are made to be $g_j = a\boldsymbol{e}_j$, which verifies $\langle g_j, g_r\rangle_{\partial X} = \delta_{jr}2a^2$. Here, $\langle\,,\,\rangle_{\partial X}$ denotes the L^2 scalar product on ∂X. Therefore, $\hat{V}_{jk}$ satisfies conditions (H1) and (H2) above.

Theorem 3.6. *Suppose that the measured dataset H^{m} satisfies (3.13), (H1) and (H2). Let ρ_* be the least-squares reconstruction in (3.9). Let the true conductivity distribution be $1 + \varepsilon\rho_r$ with $\|\rho_r\|_\infty \lesssim 1$. Then for any $\xi \in \mathbb{Z}^2$, we have*

$$\mathbb{E}|(\rho_* - \varepsilon\rho_r)^\wedge(\xi)|^2 = \frac{\sigma^2}{a^2} + O(\varepsilon^4). \tag{3.16}$$

Proof. According to the proof of theorem 3.2, we may decompose the measured data as

$$H^{\mathrm{m}}_{jk} = F_{jk}[\gamma_0] + \mathcal{D}F_{jk}(\varepsilon\rho_r) + E_{jk} + V_{jk}$$

with $\|E_{jk}\| \leqslant C\varepsilon^2$. Then the analysis in the proof is still valid if we replace E_{jk} by $E_{jk} + V_{jk}$. In particular, do so in formula (3.12) and take the mean square of both sides. Using the facts

that V_{jk} is mean zero, that $|\hat{E}_{jk}| \leqslant C\|E_{jk}\| \leqslant C\varepsilon^2$ and that $\hat{V}_{jk}$ with different indices are independent, we obtain

$$\mathbb{E}|(\rho_* - \varepsilon\rho_r)^\wedge(\xi)|^2 = \frac{1}{4a^4}((1-2(\boldsymbol{e}_1\cdot\tilde{\xi})^2)^2\mathbb{E}|\hat{V}_{11}(\xi)|^2 + 4(\boldsymbol{e}_1\cdot\tilde{\xi})^2(\boldsymbol{e}_2\cdot\tilde{\xi})^2\mathbb{E}|\hat{V}_{12}(\xi)|^2 + 4(\boldsymbol{e}_1\cdot\tilde{\xi})^2(\boldsymbol{e}_2\cdot\tilde{\xi})^2\mathbb{E}|\hat{V}_{21}(\xi)|^2 + (1-2(\boldsymbol{e}_2\cdot\tilde{\xi})^2)^2\mathbb{E}|\hat{V}_{22}(\xi)|^2) + O(\varepsilon^4).$$

Substitute (3.14) into the formula above to obtain (3.16). □

Remark 3.7. We note that (H2) is imposed so that the measurement noise dominates the truncation error but is subordinate to the deviation from a homogeneous medium. Estimate (3.16) shows that as long as the noise is small, all Fourier modes can be reconstructed sufficiently well. In other words, AEI is statistically stable with respect to additive noise.

Simple scaling shows the following. On a square with side length L and background conductivity γ_0, the right-hand side in (3.16) should be replaced by $\gamma_0^2\sigma^2 L/a^2$.

Remark 3.8. We conclude this section by showing that the pattern of two orthogonal currents is the best configuration in an averaged sense. Indeed, it is possible to choose ψ_1 and ψ_2 in (2.7) in a way that the background currents $\boldsymbol{a}_1$ and $\boldsymbol{a}_2$ satisfy $|\boldsymbol{a}_1| = |\boldsymbol{a}_2| = a$; the angle between them is $\beta \in (0,\pi)$. Let $\alpha(\xi)$ be the angle between the vector $\tilde{\xi}$ and $\tilde{\boldsymbol{a}}_1$. Then $\alpha(\xi)+\beta$ will be the angle between $\tilde{\xi}$ and $\tilde{\boldsymbol{a}}_2$. Following the calculation in lemma 3.1, we can show

$$\begin{aligned}
(\mathcal{D}F_{11}(\rho))^\wedge(\xi) &= a^2(1-2\cos^2\alpha)\hat{\rho}(\xi),\\
(\mathcal{D}F_{12}(\rho))^\wedge(\xi) &= (\mathcal{D}F_{21}(\rho))^\wedge(\xi) = a^2(\cos\beta - 2\cos\alpha\cos(\alpha+\beta))\hat{\rho}(\xi),\\
(\mathcal{D}F_{22}(\rho))^\wedge(\xi) &= a^2(1-2\cos^2(\alpha+\beta))\hat{\rho}(\xi).
\end{aligned}$$

Following the calculation in theorems 3.2 and 3.6, and using trigonometric identities, we find that

$$(\rho_* - \varepsilon\rho_r)^\wedge(\xi) \approx \frac{-\cos(2\alpha)\hat{V}_{11} - \cos(2\alpha+\beta)(\hat{V}_{12}+\hat{V}_{21}) - \cos(2\alpha+2\beta)\hat{V}_{22}}{a^2(\cos^2(2\alpha) + 2\cos^2(2\alpha+\beta) + \cos^2(2\alpha+2\beta))}.$$

We verify that the two boundary currents in the new configuration satisfy

$$\langle g_1, g_1\rangle_{\partial X} = \langle g_2, g_2\rangle_{\partial X} = 2a^2, \quad \langle g_1, g_2\rangle_{\partial X} = 2a^2\cos\beta.$$

As a result, the random variables $\hat{V}_{jk}$ are correlated in the following manner:

$$\begin{aligned}
&\mathbb{E}|\hat{V}_{jk}|^2 = 2\sigma^2a^2, \quad \text{for all } j,\ k = 1,2,\\
&\mathbb{E}\hat{V}_{11}\overline{\hat{V}_{21}} = \mathbb{E}\hat{V}_{22}\overline{\hat{V}_{12}} = 2\sigma^2a^2\cos\beta,
\end{aligned}$$

while all other pairings of noises are independent. Then we have

$$\mathbb{E}|(\rho_* - \varepsilon\rho_r)^\wedge(\xi)|^2 \approx \frac{2\sigma^2}{a^2}\frac{[\cos^2(2\alpha) + 2\cos^2(2\alpha+\beta) + \cos^2(2\alpha+2\beta)] + 2\cos^2\beta}{(\cos^2(2\alpha) + 2\cos^2(2\alpha+\beta) + \cos^2(2\alpha+2\beta))^2}.$$

It is obvious that the contribution of the second term on the numerator is minimized at $\beta = \pi/2$. In an averaged sense, the contribution of the other term is minimized also at $\beta = \pi/2$. Indeed, this is seen from the following calculation:

$$\begin{aligned}
&\frac{1}{2\pi}\int_0^{2\pi}\frac{\mathrm{d}\alpha}{\cos^2(2\alpha) + 2\cos^2(2\alpha+\beta) + \cos^2(2\alpha+2\beta)}\\
&\quad= \frac{1}{4\pi}\int_0^{2\pi}\frac{\mathrm{d}\alpha}{1+\cos^2\beta\cos(4\alpha+2\beta)}\\
&\quad= \frac{1}{2\sqrt{1-\cos^4\beta}}.
\end{aligned}$$

To summarize, the averaged effect (over frequencies) of the measurement noise is minimal when the two background currents are orthogonal.

4. The case of partial data

In this section, we consider the case when data are only obtained on a subset $X' \subset X$. This is illustrated in figure 1(b), with the shaded square representing X'.

As before, we use two illuminations at the boundary of X that generate two orthogonal constant background currents $a\boldsymbol{e}_1$ and $a\boldsymbol{e}_2$. However, the ultrasound beams only scan over X'. The data now are $\{H_{ij}(x)|x \in X'\}_{i,j=1,2}$. Since no information is provided outside X', we do not hope to reconstruct the conductivity distribution there and focus only on its restriction to X'. Following the idea of subsection 2.2, we wish to find the least-squares estimate of the minimizer of

$$J'[\gamma'] = \frac{1}{2}\int_{X'} |||F'[\gamma'] - H|||^2 \, \mathrm{d}x.$$

In this section, the 'prime' symbol is used to denote restrictions to X'. The functions F'_{jk} are defined as

$$F'_{jk}[\gamma'] = \gamma' \nabla u'_j[\gamma'] \cdot \nabla u'_k[\gamma'], \tag{4.1}$$

where u'_j, $j = 1, 2$, solves the reduced problem

$$\begin{aligned} &\nabla \cdot \gamma'(x) \nabla u'_j[\gamma'](x) = 0, \quad && x \in X', \\ &u'_j[\gamma'](x) = u_0^j(x), && x \in \partial X'. \end{aligned}$$

Here, u_0^j is the background solution over the whole domain when the jth illumination is applied. Therefore, we solve u'_j with the conductivity distribution γ' in X', and use the value of the background solution as the boundary condition at $\partial X'$.

Compare the above problem with (1.1), we observe that the reduced problem has the same form as the problem posed on the whole square. Furthermore, the boundary conditions $u'_j = u_0^j$ at $\partial X'$, $j = 1, 2$, generate two orthogonal constant currents inside X'. Consequently, the analysis we developed in the last section for the operators F_{jk}, $\mathcal{D}F_{jk}$, $\mathcal{D}F_{jk}^*$ and $\mathcal{Q}$ can be reproduced on the inner square X'. Define the corresponding operators using the 'prime'. Then the least-squares reconstruction of the contrast field inside X' is given by

$$\rho'_* = (\mathcal{Q}')^{-1} \sum_{j,k=1,2} (\mathcal{D}F'_{jk})^*(H_{jk} - F'_{jk}[\gamma_0]). \tag{4.2}$$

The following main theorem of this section shows that the above reconstruction formula captures the true medium $\gamma_r = 1 + \varepsilon\rho_r$ inside X' well enough in the L^2 sense, provided that the support of ρ_r is small and well separated from the boundary of X'.

Theorem 4.1. *Let ρ'_* be defined as in (4.2). Assume that the set $D := \{\rho_r \neq 0\}$ is well separated from the boundary, i.e. there exists a positive constant h such that the Euclidean distance $d(D, \partial X') \geqslant h$. Then we have*

$$\|\rho'_* - \varepsilon\rho_r\|_{X'} \leqslant C\big(\varepsilon^2 \|\rho_r\|_\infty^2 + \varepsilon h^{-2} \|\rho_r\|_{1,D}\big), \tag{4.3}$$

where $\|\ \|_{X'}$ is the L^2-norm on X' and $\|\ \|_{1,D}$ is the L^1-norm on D.

Remark 4.2. Note that in the case of a small inclusion, $\|\rho_r\|_{1,D}$ can be much smaller than $\|\rho_r\|_{2,D}$. Therefore, the result above shows that the optimization procedure in this section is sufficient for small inclusion detection.

Proof. First, we observe that $F'_{jk}[\gamma_0] = F_{jk}[\gamma_0]$, because in the background medium, u'_j is just the restriction to X' of u_j. Therefore, as in the proof of theorem 3.2, we have

$$\begin{aligned} H_{jk} - F'_{jk}[\gamma_0] &= H_{jk} - F_{jk}[\gamma_0] = \mathcal{D}F_{jk}(\varepsilon\rho_r) + E_{jk} \\ &= \mathcal{D}F'_{jk}(\varepsilon\rho_r) + (\mathcal{D}F_{jk} - \mathcal{D}F'_{jk})(\varepsilon\rho_r) + E_{jk}. \end{aligned}$$

Using this decomposition in (4.2), we obtain

$$\rho'_* - \varepsilon\rho_r = (\mathcal{Q}')^{-1} \sum_{j,k=1,2} (\mathcal{D}F'_{jk})^*[(\mathcal{D}F_{jk} - \mathcal{D}F'_{jk})(\varepsilon\rho_r) + E_{jk}]. \tag{4.4}$$

Since $\|E_{jk}\| \leqslant C\varepsilon^2\|\rho_r\|^2_\infty$, its contribution is well controlled. For the other term, we recall the expression of $\mathcal{D}F_{jk}$ in (3.6), and the fact that $\mathcal{D}F'_{jk}$ is defined similarly using the same background currents. It then follows

$$(\mathcal{D}F_{jk} - \mathcal{D}F'_{jk})(\rho_r) = a\boldsymbol{e}_j \cdot \nabla(v_k[\rho_r] - v'_k[\rho_r]) + a\nabla(v_j[\rho_r] - v'_j[\rho_r]) \cdot \boldsymbol{e}_k.$$

Therefore, we need to control the difference $v[\rho]$ and $v'[\rho]$ where $v[\rho]$ solves the first equation in (2.9) but with Dirichlet boundary conditions; $v'[\rho]$ solves a similar equation but on the reduced domain X'. Let $G(x, y)$ denote the Dirichlet–Green function on the whole domain X and $G'(x, y)$ the one on X'. Then we have

$$\begin{aligned}(v[\rho] - v'[\rho])(x) &= -\int_D (G(x, y) - G'(x, y))\nabla u_0(y) \cdot \nabla\rho_r(y)\,\mathrm{d}y \\ &= \int_D \nabla_y(G(x, y) - G'(x, y)) \cdot \nabla_y u_0(y)\rho_r(y)\,\mathrm{d}y.\end{aligned}$$

In the second equality, we used integration by parts and the facts that $\rho_r = 0$ on ∂D and $\Delta_y u_0 = 0$. In our setting, $\|\nabla u_0\|_\infty \leqslant C$. Hence, we have

$$\begin{aligned}\|\nabla v[\rho] - \nabla v'[\rho]\|^2_{X'} &\leqslant C\int_{X'}\int_D\int_D |\nabla_x\nabla_y R(x, y)||\nabla_x\nabla_y R(x, z)||\rho_r(y)||\rho_r(z)|\,\mathrm{d}z\,\mathrm{d}y\,\mathrm{d}x \\ &\leqslant \int_D\int_D |\rho_r(y)||\rho_r(z)|\left(\sup_{y\in D}\|\nabla_x\nabla_y R(\cdot, y)\|_{2,X'}\right)^2 \mathrm{d}y\,\mathrm{d}z.\end{aligned}$$

Here $R(x, y) = G(x - y) - G'(x, y)$. It can be written as the sum of $G - \Phi$ and $\Phi - G'$, where $\Phi(x, y)$ is the fundamental solution of the Laplace equation in $\mathbb{R}^2$. We will bound the derivative of such functions in lemma 4.3. By (4.5), we obtain

$$\|\nabla v[\rho] - \nabla v'[\rho]\|^2_{X'} \leqslant Ch^{-4}\|\rho_r\|^2_{1,D}.$$

It follows that $\|(\mathcal{D}F_{jk} - \mathcal{D}F'_{jk})(\rho_r)\|$ is bounded by $Ch^{-2}\|\rho_r\|_{1,D}$. Recall the reconstruction formula (4.4). Since $(\mathcal{Q}')^{-1}$ and $(\mathcal{D}F'_{jk})^*$ are bounded operators on L^2, the above estimate, together with the aforementioned control of E_{jk}, proves (4.3). □

We conclude this section by proving the desired gradient estimate for the difference of the Green functions.

Lemma 4.3. *Let $\Phi(x, y) = -\frac{1}{2\pi}\log|x-y|$ be the fundamental solution of the Laplace equation in $\mathbb{R}^2$, and let $G(x, y)$ be the Dirichlet–Green function on some connected and bounded domain Y with smooth boundary. Let D be a set with smooth boundary such that the Euclidean distance $d(D, \partial Y) > h$ for some positive number h. Then for any $p \geqslant 1$, there exists some finite constant $C(p)$ so that*

$$\sup_{y\in D}\|\nabla_x\nabla_y G(\cdot, y) - \nabla_x\nabla_y\Phi(\cdot, y)\|_{p,Y} \leqslant C(p)h^{-2}. \tag{4.5}$$

Proof. The Green function is in fact constructed as $G(x, y) = \Phi(x, y) + \phi(x, y)$, with ϕ satisfying

$$\begin{aligned}&\Delta_x\phi(x, y) = 0, \quad x \in Y, \\ &\phi(x, y) = -\Phi(x, y), \quad x \in \partial Y.\end{aligned}$$

Set D_r for r sufficiently small to be the set consisting of points whose distance from D is less than r, i.e. $D_r = \{x : d(x, D) \leqslant r\}$. Choose some smooth cut-off function $\varphi_h(x)$ so that $\varphi_h \equiv 1$ on $D_{h/2}^c$ and φ_h vanishes inside $D_{h/4}$ and outside a sufficiently large ball containing Y. Furthermore, assume that $0 \leqslant \varphi_h(x) \leqslant 1$ holds everywhere. Then $\varphi_h(\cdot)G(\cdot, y)$ is a smooth function on X. In particular, we have

$$\phi(x, y) = \varphi_h(x)\Phi(x, y) + R_1(x, y), \tag{4.6}$$

where R_1 solves

$$\Delta_x R_1(x, y) = -\Delta_x(\varphi_h(x)\Phi(x, y)), \quad x \in Y,$$

and $R_1(\cdot, y) = 0$ on the boundary ∂Y.

Let $y \in D$, then $\varphi_h(x)G(x, y)$ is smooth on $Y \times D$ because when $x \in D$ the function vanishes. Therefore, we can differentiate the above equation to obtain

$$\begin{aligned} &\Delta_x \nabla_y R_1(x, y) = -\Delta_x(\varphi_h(x)\nabla_y\Phi(x, y)), \quad x \in Y, \\ &\nabla_y R_1(x, y) = 0, \quad x \in \partial Y. \end{aligned} \tag{4.7}$$

Then from the standard theory of elliptic equations together with the fact that $\Delta_x\nabla_y\Phi$ vanishes on the support of φ_h, we have, for any fixed $y \in D$,

$$\|\nabla_y R_1(\cdot, y)\|_{W^{2,2}(Y)} \leqslant C(\|\Delta_x\varphi_h(\cdot)\nabla_y\Phi(\cdot, y)\| + 2\|\nabla_x\varphi_h \cdot \nabla_x\nabla_y\Phi(\cdot, y)\|). \tag{4.8}$$

Note that $\nabla_x\varphi_h$ (and hence $\Delta_x\varphi_h$) is supported on the domain $D_{h/2}\backslash D_{h/4}$. For any x in this set and any $y \in D$, we have

$$|\nabla_y\Phi(x, y)| \leqslant Ch^{-1}, \qquad |\nabla_x\nabla_y\Phi(x, y)| \leqslant Ch^{-2}. \tag{4.9}$$

Recall the definition of φ_h. It is possible to construct φ_h by shifting and scaling some standard cutoff function φ whose $W^{2,q}$ norm is bounded for any $1 \leqslant q \leqslant \infty$. Then from a scaling argument, we have

$$\|\nabla\varphi_h\|_q \leqslant Ch^{\frac{d}{q}-1}, \qquad \|\Delta\varphi_h\|_q \leqslant Ch^{\frac{d}{q}-2}. \tag{4.10}$$

Here, $d = 2$ is the dimension of Y. Hence, the right-hand side of (4.8) is bounded by

$$\|\nabla_y\Phi(x, y)\|_{\infty,\mathrm{supp}\nabla_x\varphi}\|\Delta_x\varphi_h\|_{L^2} + 2\|\nabla_x\nabla_y\Phi(x, y)\|_{\infty,\mathrm{supp}\nabla_x\varphi}\|\nabla_x\varphi_h\|_{L^2} \leqslant Ch^{-2}.$$

This shows that $\|\nabla_x\nabla_y R_1(\cdot, y)\|_{W^{1,2}} \leqslant Ch^{-2}$. By the Sobolev embedding theorem, for any $1 \leqslant p < \infty$, there exists some constant $C(p)$ so that $\|\nabla_x\nabla_y R_1(x, y)\|_p \leqslant C(p)h^{-2}$. From the decomposition of $\phi(x, y) = G(x, y) - \Phi(x, y)$ in (4.6), we have

$$\nabla_x\nabla_y\phi(x, y) = \nabla_x\varphi_h \otimes \nabla_y\Phi(x, y) + \varphi_h\nabla_x\nabla_y\Phi + \nabla_x\nabla_y R_1(x, y). \tag{4.11}$$

We have estimated the L^p bound of the last term above. The other two terms in the decomposition can be bounded by simply using (4.9) and (4.10) and the fact that they are non-zero only for $x \in \mathrm{supp}\nabla\varphi_h$. It turns out that they are of order h^{-2}. This completes the proof. □

5. The case of limited-view data

In the previous sections, boundary conditions which generate orthogonal background currents are used for AEI. Such a setting requires all four sides of the square to be accessible. In this section, we consider 'a very limited-view' case in which only the top side of the square is accessible, as illustrated in figure 2. On the other sides, therefore, zero-flux conditions, i.e. homogeneous Neumann boundary conditions, are imposed.

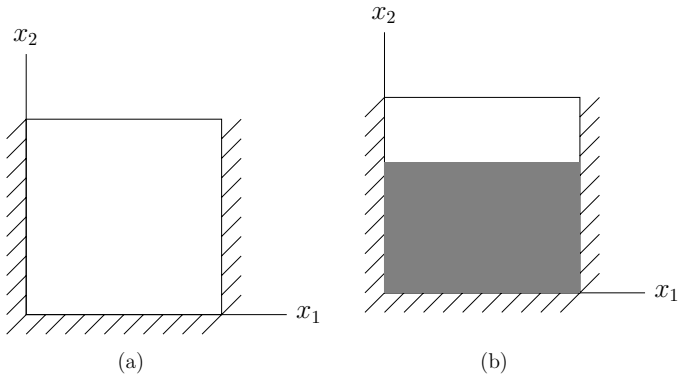

Figure 2. (a) The unit square domain in the limited-view case. The shaded sides are not accessible. (b) Two conductivity phases separated by an interface.

Without loss of generality, we assume that the background conductivity is $\gamma_0 = 1$. For any positive integer k,

$$u_0(x_1, x_2) = \frac{1}{k\pi} \cos k\pi x_1 \cosh k\pi x_2$$

is a solution in the background medium. In fact, we check that

$$\nabla u_0 = \begin{pmatrix} -\sin k\pi x_1 \cosh k\pi x_2 \\ \cos k\pi x_1 \sinh k\pi x_2 \end{pmatrix}, \qquad |\nabla u_0|^2 = \frac{\cosh 2k\pi x_2 - \cos 2k\pi x_1}{2}.$$

In particular, this shows that u_0 satisfies the zero-flux conditions on the inaccessible sides. Also, $u_0(x_1, x_2)$ is yielded by injecting a current $g(x) = \cos k\pi x_1 \sinh k\pi$ from the top. The aim of this section is to investigate whatever information can be extracted in this very limited-view situation.

Define $F[\gamma] = \gamma|\nabla u[\gamma]|^2$. According to (2.11), the Fréchet derivative $\mathcal{D}F$ at γ_0 operated on ρ, i.e. $\mathcal{D}F(\rho)$, is given by

$$\frac{\rho(\cosh 2k\pi x_2 - \cos 2k\pi x_1)}{2} - 2 \sin k\pi x_1 \cosh k\pi x_2 \frac{\partial v[\rho]}{\partial x_1} + 2 \cos k\pi x_1 \sinh k\pi x_2 \frac{\partial v[\rho]}{\partial x_2}.$$

Extend the functions ρ, $v[\rho]$ and $\mathcal{D}F(\rho)$ evenly in x_1 to the domain $(-1, 1) \times (0, 1)$. For each fixed depth x_2, let $\hat{f}(n, x_2)$ be the Fourier coefficients in x_1, i.e.

$$\hat{f}(n, x_2) = \frac{1}{2} \int_{-1}^{1} f(x_1, x_2)\, \mathrm{e}^{-\mathrm{i}\pi n x_1}\, \mathrm{d}x_1. \tag{5.1}$$

Then the Fourier coefficients (in x) of $\mathcal{D}F(\rho)$ is characterized in the following lemma.

Lemma 5.1. *The Fourier coefficients of $\mathcal{D}F(\cdot, x_2)$ can be written as*

$$\begin{aligned}(\mathcal{D}F(\rho))^\wedge(m, x_2) = {} & \frac{1}{2}(I - \mathcal{L}_0)\hat{\rho}(m, x_2) + \left(-\frac{\cosh 2k\pi x_2}{4} I + \mathcal{L}_-\right)\hat{\rho}(m - 2k, x_2) \\ & + \left(-\frac{\cosh 2k\pi x_2}{4} I + \mathcal{L}_+\right)\hat{\rho}(m + 2k, x_2).\end{aligned} \tag{5.2}$$

Here, $\mathcal{L}_0$, $\mathcal{L}_-$ and $\mathcal{L}_+$ are integral operators in y with uniformly bounded integral kernels.

The proof of this lemma is a lengthy calculation which is given in the appendix. Since the integral operators above are smoothing, we expect that the singular parts of $(\mathcal{D}F(\rho))^\wedge$ above can detect singularity of ρ in the vertical direction. Take the approximation

$$(\mathcal{D}F(\rho))^\wedge(m, x_2) \approx \frac{1}{2}\hat{\rho}(m, x_2) - \frac{\cosh 2k\pi x_2}{4}\hat{\rho}(m - 2k, x_2) - \frac{\cosh 2k\pi x_2}{4}\hat{\rho}(m + 2k, x_2).$$

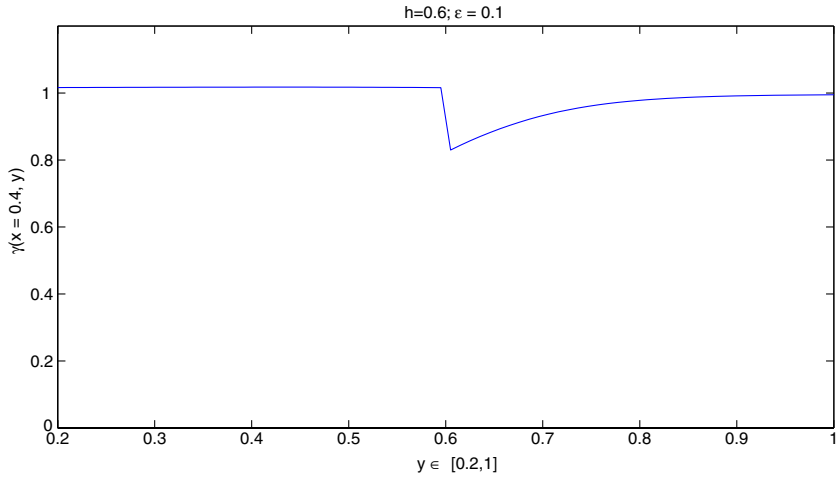

Figure 3. Reconstruction of an interface from limited-view data.

The right-hand side above is a convolution in the Fourier domain. It corresponds to

$$\mathcal{D}F(\rho) \approx \tfrac{1}{2}(1 - \cos 2k\pi x_1 \cosh 2k\pi x_2)\rho.$$

Since $\mathcal{D}F$ is self-adjoint, we have

$$\mathcal{D}F^*\mathcal{D}F(\rho) \approx \tfrac{1}{4}(1 - \cos 2k\pi x_1 \cosh 2k\pi x_2)^2\rho.$$

This function is not invertible on the curve $\cos 2k\pi x_1 \cosh 2k\pi x_2 = 1$. To bypass this difficulty, we may use another current $g_2 = \cos 2k\pi x_1 \sinh 2k\pi$ on the top side of square. Denote the corresponding data function as F_2. The above calculation applies and we have

$$\mathcal{D}F_2^*\mathcal{D}F_2(\rho) \approx \tfrac{1}{4}(1 - \cos 4k\pi x_1 \cosh 4k\pi x_2)^2\rho.$$

Suppose we minimize the discrepancy between the two datasets, i.e. $\alpha_1\|F_1[\gamma] - H_1\|^2 + \alpha_2\|F_2[\gamma] - H_2\|^2$, where α_1 and α_2 are weight parameters to balance the two terms. Then the least-squares solution is approximated by $\gamma_0 + \rho_*$ where

$$\alpha_1(\mathcal{D}F_1^*\mathcal{D}F_1 + \alpha_2\mathcal{D}F_2^*\mathcal{D}F_2)\rho_* = \alpha_1\mathcal{D}F_1^*(H_1 - F_1[\gamma_0]) + \alpha_2\mathcal{D}F_2^*(H_2 - F_2[\gamma_0]). \tag{5.3}$$

It is easy to check that $1 - \cos 2k\pi x_1 \cosh 2k\pi x_2$ and $1 - \cos 4k\pi x_1 \cosh 4k\pi x_2$ do not vanish simultaneously except at the two bottom corners $(0, 0)$ and $(1, 0)$. Therefore, if we set $\alpha_1 = 1$ and $\alpha_2 = \alpha$, for any depth $1 - x_2 < 1$, the reconstruction formula is given by

$$\gamma(x_1, x_2) = \gamma_0 + \frac{2\sum_{j=1}^{2}\alpha_j(1 - \cos 2jk\pi x_1 \cosh 2jk\pi x_2)\{H_j(x_1, x_2) - F_j[\gamma_0]\}}{\sum_{j=1}^{2}\alpha_j(1 - \cos 2jk\pi x_1 \cosh 2jk\pi x_2)^2}. \tag{5.4}$$

Remark 5.2. To test the performance of (5.4), we apply it to the case when $\gamma(x_1, x_2) = 1 + \varepsilon\chi_{x_2<h}(x_1, x_2)$, where χ is the characteristic function of a set (see figure 2). The body X hence contains two phases with an interface at $x_2 = h$. In this simple setting, the expression of $H_j = \gamma|\nabla u_j[\gamma]|^2$ is explicit, and the point-wise formula (5.4) can be calculated directly.

In a numerical experiment, we set $\varepsilon = 0.1$, $h = 0.6$ and $\alpha = \cosh(2\pi)/\cosh(4\pi)$, and apply the formula to the vertical line $x_1 = 0.5, 0 < x_2 < 1$. Then the interface can clearly be seen from the reconstruction given by (5.4); see figure 3. The value γ_* is indeed greater than 1 for $x_2 < h$, but the deviation from γ_0 is smaller than expected; furthermore, the drop of γ_*

across the interface is greater than the true value. As h and x_1 vary, these features do not change dramatically. To summarize, the proposed formula detects the interface at h sufficiently well.

Of course, the reconstruction formula above does not work for general conductivity distributions. More delicate utilization of the Fourier modes captured in lemma 5.1 may help, but this is not at all simple and is beyond the scope of this paper.

6. Conclusion

In this paper, evidence of resolution enhancement due to internal measurements for conductivity imaging has been given. A resolution and stability analysis has been provided for acousto-electric imaging with full data. Moreover, the effect of partial or limited-view data on image reconstruction has been quantified in the presence of measurement noise. It has been observed that the limited-view aspect affects the image quality much more significantly than partial data. The conclusions of this paper hold only under the assumption that the noise is measurement noise. For medium noise or clutter, the situation is quite different and more involved.

Acknowledgment

This work was supported by the ERC Advanced grant project MULTIMOD–267184.

Appendix. Derivation of lemma 5.1

In this section, we record the lengthy calculation which leads to (5.2). The integral kernels associated with the integral operators $\mathcal{L}_0$, $\mathcal{L}_-$ and $\mathcal{L}_+$ are given by the functions L_0, L_- and L_+.

The function $v[\rho]$ in the expression of $\mathcal{D}F(\rho)$ satisfies

$$\Delta v[\rho] = \sin k\pi x_1 \ \cosh k\pi x_2 \frac{\partial \rho}{\partial x_1} - \cos k\pi x_1 \ \sinh k\pi x_2 \frac{\partial \rho}{\partial x_2},$$

on the unit square with zero flux on the three shaded sides as shown in figure 2.

To solve this equation, we extend the functions ρ and $v[\rho]$ evenly in x_1 to the domain $(-1, 1) \times (0, 1)$. This takes care of the Neumann condition on the left and right sides. Let $(v[\rho])^\wedge(n, x_2)$ for n denote a typical Fourier coefficient of $v[\rho](\cdot, x_2)$. Then we have

$$\begin{aligned}\frac{\partial^2}{\partial x_2^2}(v[\rho])^\wedge(n, x_2) - (n\pi)^2(v[\rho])^\wedge(n, x_2) = {} & \frac{(n-k)\pi}{2} \cosh k\pi x_2 \ \hat{\rho}(n-k, x_2) \\ & - \frac{(n+k)\pi}{2} \cosh k\pi x_2 \ \hat{\rho}(n+k, x_2) - \frac{1}{2} \sinh k\pi x_2 \frac{\partial \hat{\rho}}{\partial x_2}(n-k, x_2) \\ & - \frac{1}{2} \sinh k\pi x_2 \frac{\partial \hat{\rho}}{\partial x_2}(n+k, x_2), \end{aligned} \tag{A.1}$$

with the boundary condition

$$-\frac{\partial}{\partial x_2}(v[\rho])^\wedge(n, 0) = \frac{\partial}{\partial x_2}(v[\rho])^\wedge(n, 1) = 0.$$

Take Fourier coefficients in the expression of $\mathcal{D}F(\rho)$. We have

$$\begin{aligned}(\mathcal{D}F(\rho))^\wedge(m, x_2) = {} & \frac{\cosh 2k\pi x_2}{2} \hat{\rho}(m, x_2) - \frac{1}{4}\hat{\rho}(m-2k, x_2) - \frac{1}{4}\hat{\rho}(m+2k, x_2) \\ & - (m-k)\pi \cosh k\pi x_2 \ (v[\rho])^\wedge(m-k) + (m+k)\pi \cosh k\pi x_2 (v[\rho])^\wedge(m+k) \\ & + \sinh k\pi x_2 \frac{\partial}{\partial x_2}(v[\rho])^\wedge(m-k, x_2) + \sinh k\pi x_2 \frac{\partial}{\partial x_2}(v[\rho])^\wedge(m+k, x_2). \end{aligned}$$

Abuse notation and make the dependence on x_2, k implicit when it is convenient. We can rewrite the above formula as

$$(\mathcal{D}F(\rho))^\wedge(m, x_2) = Q_0(m, x_2)\hat{\rho}(m) + Q_-(m, x_2)\hat{\rho}(m-2k) + Q_+(m, x_2)\hat{\rho}(m+2k).$$

The task now is to find explicit expressions for the operators Q_0, Q_- and Q_+.

When $n \neq 0$, the Green function $G(\tau, \tau_0; n)$ associated with this equation is

$$\partial_\tau^2 G(\tau, \tau_0; n) - (n\pi)^2 G(\tau, \tau_0; n) = \delta_{\tau_0}(\tau),$$

with the Neumann boundary condition at the two ends. The solution to this equation has the expression

$$G(\tau, \tau_0; n) = \begin{cases} -\dfrac{\cosh n\pi(1-\tau_0)\cosh n\pi\tau}{n\pi \sinh n\pi}, & \tau < \tau_0, \\ -\dfrac{\cosh n\pi\tau_0 \cosh n\pi(1-\tau)}{n\pi \sinh n\pi}, & \tau \geqslant \tau_0. \end{cases}$$

The Green function is continuous and symmetric. Its derivative with respect to τ is

$$\Gamma_1(\tau, \tau_0; n) = \frac{\partial}{\partial\tau}G = \begin{cases} -\dfrac{\cosh n\pi(1-\tau_0)\ \sinh n\pi\tau}{\sinh n\pi}, & \tau < \tau_0, \\ \dfrac{\cosh n\pi\tau_0\ \sinh n\pi(1-\tau)}{\sinh n\pi}, & \tau \geqslant \tau_0. \end{cases}$$

Its derivative with respect to τ_0 is

$$\Gamma_2(\tau, \tau_0; n) = \frac{\partial}{\partial\tau_0}G = \begin{cases} \dfrac{\sinh n\pi(1-\tau_0)\ \cosh n\pi\tau}{\sinh n\pi}, & \tau < \tau_0, \\ -\dfrac{\sinh n\pi\tau_0\ \cosh n\pi(1-\tau)}{\sinh n\pi}, & \tau \geqslant \tau_0. \end{cases}$$

The solution to (A.1) is given by

$$\begin{aligned}(v[\rho])^\wedge(n, x_2) = \int_0^1 G(x_2, \tau_0) \Bigg(& \frac{(n-k)\pi}{2}\cosh k\pi\tau_0\ \hat{\rho}(n-k, \tau_0) \\ & -\frac{(n+k)\pi}{2}\cosh k\pi\tau_0\ \hat{\rho}(n+k, \tau_0) - \frac{1}{2}\sinh k\pi\tau_0 \frac{\partial\hat{\rho}}{\partial x_2}(n-k, \tau_0) \\ & -\frac{1}{2}\sinh k\pi\tau_0 \frac{\partial\hat{\rho}}{\partial x_2}(n+k, \tau_0)\Bigg)\,\mathrm{d}\tau_0.\end{aligned}$$

Integrating by parts, we rewrite the above as

$$\begin{aligned}(v[\rho])^\wedge(n, x_2) = & \int_0^1 \frac{n\pi G(x_2, \tau_0; n)\cosh k\pi\tau_0 + \Gamma_2(x_2, \tau_0; n)\sinh k\pi\tau_0}{2}\hat{\rho}(n-k, \tau_0)\,\mathrm{d}\tau_0 \\ & + \int_0^1 \frac{-n\pi G(x_2, \tau_0; n)\cosh k\pi\tau_0 + \Gamma_2(x_2, \tau_0; n)\sinh k\pi\tau_0}{2}\hat{\rho}(n+k, \tau_0)\,\mathrm{d}\tau_0.\end{aligned}$$

To obtain the derivative of $(v[\rho])^\wedge$ in x_2, we take derivatives under the integral sign on the above expression. Note that this should be done on separated intervals because Γ_2 is not continuous along the diagonal. We obtain

$$\begin{aligned}\frac{\partial(v[\rho])^\wedge}{\partial x_2}(n, x_2) = & n\pi\int_0^1 \frac{\Gamma_1(x_2, \tau_0; n)\cosh k\pi\tau_0 + \Gamma_3(x_2, \tau_0; n)\sinh k\pi\tau_0}{2}\hat{\rho}(n-k, \tau_0)\,\mathrm{d}\tau_0 \\ & + n\pi\int_0^1 \frac{-\Gamma_1(x_2, \tau_0; n)\cosh k\pi\tau_0 + \Gamma_3(x_2, \tau_0; n)\sinh k\pi\tau_0}{2}\hat{\rho}(n+k, \tau_0)\,\mathrm{d}\tau_0 \\ & - \frac{\sinh n\pi x_2\ \cosh n\pi(1-x_2)\ \sinh k\pi x_2}{2\sinh n\pi}(\hat{\rho}(n-k) + \hat{\rho}(n+k)) \\ & - \frac{\sinh n\pi(1-x_2)\ \cosh n\pi x_2\ \sinh k\pi x_2}{2\sinh n\pi}(\hat{\rho}(n-k) + \hat{\rho}(n+k)).\end{aligned}$$

Above, we have used the notation

$$\Gamma_3(x_2,\tau_0;n)=\frac{1}{n\pi}\frac{\partial}{\partial x_2}\Gamma_2=\begin{cases}\dfrac{\sinh n\pi(1-\tau_0)\ \sinh n\pi x_2}{\sinh n\pi}, & x_2<\tau_0,\\ \dfrac{\sinh n\pi y_0\ \sinh n\pi(1-x_2)}{\sinh n\pi}, & x_2\geqslant\tau_0.\end{cases}$$

A further simplification shows

$$\begin{aligned}\frac{\partial(v[\rho])^\wedge}{\partial x_2}&=n\pi\int_0^1\frac{\Gamma_1(x_2,\tau_0;n)\cosh k\pi\tau_0+\Gamma_3(x_2,\tau_0;n)\sinh k\pi\tau_0}{2}\hat\rho(n-k,\tau_0)\,\mathrm{d}\tau_0\\&\quad+n\pi\int_0^1\frac{-\Gamma_1(x_2,\tau_0;n)\cosh k\pi\tau_0+\Gamma_3(x_2,\tau_0;n)\sinh k\pi\tau_0}{2}\hat\rho(n+k,\tau_0)\,\mathrm{d}\tau_0\\&\quad-\frac{1}{2}\sinh k\pi x_2(\hat\rho(n-k)+\hat\rho(n+k)).\end{aligned}$$

Now recall the expression of $(\mathcal{D}F(\rho))^\wedge$ and collect terms. We find

$$\begin{aligned}Q_0\hat\rho&=\left(\frac{\cosh 2k\pi x_2}{2}-\sinh^2 k\pi x_2\right)\hat\rho(m,x_2)\\&\quad-\frac{(m-k)\pi\cosh k\pi x_2}{2}\int_0^1(-\Gamma_0(m-k)\cosh k\pi\tau_0+\Gamma_2(m-k)\sinh k\pi\tau_0)\hat\rho(m)\,\mathrm{d}\tau_0\\&\quad+\frac{(m+k)\pi\cosh k\pi x_2}{2}\int_0^1(\Gamma_0(m+k)\cosh k\pi\tau_0+\Gamma_2(m+k)\sinh k\pi\tau_0)\hat\rho(m)\,\mathrm{d}\tau_0\\&\quad+\frac{(m-k)\pi\sinh k\pi x_2}{2}\int_0^1(-\Gamma_1(m-k)\cosh k\pi\tau_0+\Gamma_3(m-k)\sinh k\pi\tau_0)\hat\rho(m)\,\mathrm{d}\tau_0\\&\quad+\frac{(m+k)\pi\sinh k\pi x_2}{2}\int_0^1(\Gamma_1(m+k)\cosh k\pi\tau_0+\Gamma_3(m+k)\sinh k\pi\tau_0)\hat\rho(m)\,\mathrm{d}\tau_0.\end{aligned}$$

Above, $\Gamma_0(x_2,\tau_0;n)$ is short for $n\pi G(x_2,\tau_0;n)$. We further simplify the above expression to

$$Q_0\hat\rho(m,x_2)=\frac{1}{2}(I-\mathcal{L}_0)\hat\rho(m,x_2)=\frac{1}{2}\left(\hat\rho(m,x_2)-\int_0^1 L_0(x_2,\tau_0;m)\hat\rho(m,\tau_0)\mathrm{d}\tau_0\right).\quad(A.2)$$

The integral kernel is given by

$$\begin{aligned}L_0(x_2,\tau_0;m)&=\frac{(m-k)\pi}{\sinh(m-k)\pi}\cosh[(m-k)\pi-(m-2k)\pi\tau_0]\cosh(m-2k)x_2\\&\quad+\frac{(m+k)\pi}{\sinh(m+k)\pi}\cosh[(m+k)\pi-(m+2k)\pi\tau_0]\cosh(m+2k)x_2,\end{aligned}$$

for $x_2<\tau_0$ and when $x_2\geqslant\tau_0$ it becomes

$$\begin{aligned}L_0(x_2,\tau_0;m)&=\frac{(m-k)\pi}{\sinh(m-k)\pi}\cosh(m-2k)\tau_0\cosh[(m-k)\pi-(m-2k)\pi x_2]\\&\quad+\frac{(m+k)\pi}{\sinh(m+k)\pi}\cosh(m+2k)\tau_0\cosh[(m+k)\pi-(m+2k)\pi x_2].\end{aligned}$$

Now, we collect the terms that contribute to Q_-. We have

$$\begin{aligned}Q_-(\hat\rho(m-2k,x_2))&=\left(-\frac{1}{4}-\frac{1}{2}\sinh^2 k\pi x_2\right)\hat\rho(m-2k,x_2)\\&\quad-\cosh k\pi x_2\int_0^1\frac{\Gamma_0(x_2,\tau_0;m-k)\cosh k\pi\tau_0+\Gamma_2(x_2,\tau_0;m-k)\sinh k\pi\tau_0}{2((m-k)\pi)^{-1}}\\&\quad\times\hat\rho(m-2k,\tau_0)\,\mathrm{d}\tau_0\end{aligned}$$

$$+ \sinh k\pi x_2 \int_0^1 \frac{\Gamma_1(x_2, \tau_0; m-k)\cosh k\pi\tau_0 + \Gamma_3(x_2, \tau_0; m-k)\sinh k\pi\tau_0}{2((m-k)\pi)^{-1}} \times \hat{\rho}(m-2k, \tau_0)\,\mathrm{d}\tau_0.$$

We can rewrite the above expression as

$$Q_-(\hat{\rho}(m-2k, x_2)) = -\frac{\cosh 2k\pi x_2}{4}\hat{\rho}(m-2k, x_2) + \int_0^1 L_-(x_2, \tau_0; m)\hat{\rho}(m-2k, \tau_0)\,\mathrm{d}\tau_0. \tag{A.3}$$

The integral kernel is given by

$$L_-(x_2, \tau_0; m) = \frac{(m-k)\pi}{\sinh(m-k)\pi}\begin{cases}\cosh[(m-k)\pi - m\pi\tau_0]\ \cosh(m-2k)\pi x_2, & x_2 < \tau_0;\\ \cosh m\pi\tau_0\ \cosh[(m-k)\pi - (m-2k)\pi x_2], & x_2 \geqslant \tau_0.\end{cases}$$

Note that L_- is not continuous along the diagonal.

Finally, we collect the terms for Q_+. We have

$$\begin{aligned}Q_+(\hat{\rho}(m+2k, x_2)) = {} & \left(-\frac{1}{4} - \frac{1}{2}\sinh^2 k\pi x_2\right)\hat{\rho}(m+2k, x_2)\\ & + \cosh k\pi x_2 \int_0^1 \frac{-\Gamma_0(x_2, \tau_0; m+k)\cosh k\pi\tau_0 + \Gamma_2(x_2, \tau_0; m+k)\sinh k\pi\tau_0}{2((m+k)\pi)^{-1}} \\ & \times \hat{\rho}(n+2k, \tau_0)\,\mathrm{d}\tau_0\\ & + \sinh k\pi x_2 \int_0^1 \frac{-\Gamma_1(x_2, \tau_0; m+k)\cosh k\pi\tau_0 + \Gamma_3(x_2, \tau_0; m+k)\sinh k\pi\tau_0}{2((m+k)\pi)^{-1}} \\ & \times \hat{\rho}(n+2k, \tau_0)\,\mathrm{d}\tau_0.\end{aligned}$$

We can rewrite the above expression as

$$Q_+(\hat{\rho}(m+2k, x_2)) = -\frac{\cosh 2k\pi x_2}{4}\hat{\rho}(m+2k, x_2) + \int_0^1 L_+(x_2, \tau_0; m)\hat{\rho}(m+2k, \tau_0)\,\mathrm{d}\tau_0. \tag{A.4}$$

The integral kernel is given by

$$L_+(x_2, \tau_0; m) = \frac{(m+k)\pi}{\sinh(m+k)\pi}\begin{cases}\cosh[(m+k)\pi - m\pi\tau_0]\ \cosh(m+2k)\pi x_2, & x_2 < \tau_0;\\ \cosh m\pi\tau_0\ \cosh[(m+k)\pi - (m+2k)\pi x_2], & x_2 \geqslant \tau_0.\end{cases}$$

Note that L_+ is not continuous along the diagonal.

So far, we did not consider the case when $n = 0$. For this case, the Green function of the $(v[\rho])^\wedge$ needs to be modified. The source δ_{τ_0} is not consistent with the zero Neumann boundary condition and should be replaced by $\delta_{\tau_0} - 1$. Then we have

$$G(\tau, \tau_0; 0) = \begin{cases}\dfrac{1}{6} - \dfrac{\tau^2 + (1-\tau_0)^2}{2}, & \tau < \tau_0,\\ \dfrac{1}{6} - \dfrac{(1-\tau)^2 + \tau_0^2}{2}, & \tau \geqslant \tau_0.\end{cases}$$

The corresponding expressions for Q_0, Q_- and Q_+ can be found following the same calculation above. Although the calculation in this case is simpler, the expressions are still lengthy and we do not present them here. Nevertheless, we reiterate that the singular part of the operators Q does not change.

References

[1] Ammari H 2008 *An Introduction to Mathematics of Emerging Biomedical Imaging* (*Mathematics and Applications* vol 62) (Berlin: Springer)

[2] Ammari H, Bonnetier E, Capdeboscq Y, Tanter M and Fink M 2008 Electrical impedance tomography by elastic deformation *SIAM J. Appl. Math.* **68** 1557–73

[3] Ammari H, Capdeboscq Y, De Gournay F, Rozanova-Pierrat A and Triki F 2011 Microwave imaging by elastic deformation *SIAM J. Appl. Math.* **71** 2112–30

[4] Ammari H, Garnier J, Jing W and Nguyen L 2012 Quantitative thermo-acoustic imaging: an exact reconstruction formula submitted

[5] Ammari H, Garnier J and Sølna K 2012 Resolution and stability analysis in full-aperture, linearized conductivity and wave imaging *Proc. Am. Math. Soc.* at press

[6] Ammari H, Garnier J and Sølna K 2012 Limited view resolving power of conductivity imaging from boundary measurements submitted

[7] Bal G, Bonnetier F, Monard F and Triki F 2011 Inverse diffusion from knowledge of power densities submitted

[8] Bal G and Monard F 2011 Inverse diffusion problem with redundant internal information submitted

[9] Capdeboscq Y, Fehrenbach J, de Gournay F and Kavian O 2009 Imaging by modification: numerical reconstruction of local conductivities from corresponding power density measurements *SIAM J. Imaging Sci.* **2** 1003–30

[10] Gebauer B and Scherzer O 2008 Impedance-acoustic tomography *SIAM J. Appl. Math.* **69** 565–76

[11] Kuchment P and Kunyansky L 2010 Synthetic focusing in ultrasound modulated tomography *Inverse Problems Imaging* **4** 665–73

[12] Kuchment P and Kunyansky L 2011 2D and 3D reconstructions in acousto-electric tomography *Inverse Problems* **27** 055013

[13] Kuchment P and Steinhauer D 2011 Stabilizing inverse problems by internal data submitted

[14] Monard F and Bal G 2011 Inverse anisotropic diffusion from power density measurements in two dimensions submitted

[15] Seo J K and Woo E J 2011 Magnetic resonance electrical impedance tomography (MREIT) *SIAM Rev.* **53** 40–68

[16] Triki F 2010 Uniqueness and stability for the inverse medium problem with internal data *Inverse Problems* **26** 095014

[17] Zhang H and Wang L 2004 Acousto-electric tomography *Proc. SPIE* **5320** 145–9